Desalination and Water Treatment
www.deswater.com

doi:10.5004/dwt.2018.23154

132 (2018) 253–262
November

Preparation of a novel two-dimensional carbon material and enhancing Pb(II) removal by tri-isopropanolamine

Xin Wen[a,b], Zhanfang Cao[a,b,*], Jing Wang[a,b], Shuai Wang[a,b], Hong Zhong[a,b,*]

[a]*College of Chemistry and Chemical Engineering, Central South University, Changsha 410083, Hunan,China, email: 27297333@qq.com (X. Wen), zfcaocsu@163.com (Z. Cao), 407052560@qq.com (J. Wang),*
[b]*Hunan Provincial Key Laboratory of Efficient and Clean Utilization of Manganese Resources, Central South University, Changsha 410083, Hunan, China, email: wangshuai@csu.edu.cn (S. Wang), huagongyejin@163.com (H. Zhong)*

Received 16 April 2018; Accepted 17 September 2018

ABSTRACT

A novel tri-isopropanolamine functionalized graphene oxide (TI-GO) adsorbent was synthesized by one-step reaction at 358K. Then the prepared TI-GO was characterized by SEM-EDS, FTIR, Raman spectra, TG, BET and XPS. The characterization results indicated the TI-GO has been synthesized successfully and it interact with Pb(II) ions through its nitrogen and oxygen-containing functional groups. Batch adsorption experiments were applied to evaluate the optimized conditions of adsorption. The results indicated that the TI-GO can reach equilibrium adsorption in 30 min and get maximum adsorption capacity at 293 K, pH 5.0. Besides, the adsorption kinetic and adsorption isotherm research indicated that the adsorption of TI-GO fit pseudo-second-order (PSO) kinetic and Langmuir adsorption isotherm model. In addition, the maximum adsorption capacity evaluated by Langmuir adsorption isotherm equation is 1478 mg/g.

Keywords: Adsorption; Graphene oxide; Lead ion; Tri-isopropanolamine

1. Introduction

With the development of modern industry, heavy metal pollution of aqueous solutions due to the discharge of industrial waste water has become a global environmental problem [1]. Heavy metal ions will be accumulated in the aquatic organisms and adsorbed by body through food chain [2]. Pb(II) ions is a common heavy metal ion in aqueous solutions. It will cause serious varieties of problems, including kidney disease, anaemia and mental retardation [3]. Considering its severe toxicity, it is of great significance to develop an effective method for the removal of Pb(II) ions from waste water. Many methods were applied including flocculation [4], chemical precipitation [5], electrochemical methodology [6], co-precipitation [7], membrane filtration [8], ion exchange [9] and adsorption [10]. Among the treatment methods mentioned above, adsorption is the most widely used technique which can remove Pb(II) ions effectively considering its low cost and high efficiency [11–12].

Nowadays, there are many adsorbents have been applied for the removal of heavy metal ions including carbon nanotubes [13–16], nanoparticles and nanocomposites [17,18]. But these materials have some shortcomings such as restricted adsorption conditions and limited adsorption capacity. To solve these problems, graphene oxide (GO) has become research focus because of its large specific surface area, low mass density and various oxygen-containing functional groups [19,20], such as hydroxyl, carboxyl and epoxy [21]. It not only can significantly enhance its dispersion property in aqueous solutions but also modify GO as a superior adsorbents for the removal of Pb(II) ions.

As we known, the adsorption capacity is usually influenced by the surface functional groups of adsorbent. Since GO sheets contain lots of reactive oxygen-containing functional groups, which means GO is a superior fundamental

*Corresponding author.

material for the immobilization of various substances onto its surface [22,23]. Yan et al. [24] combined GO with chitosan to improve the adsorption capacity for metal ions and increase its pH range. Shao et al. [25] functionalized GO with amidoxime for the removal of U(VI) since its abundant hydroxyl and amino functional groups. Therefore, increasing the oxygen-containing functional groups of GO by combining it with molecule, which possesses abundant oxygen-containing groups and amino functional groups can improve its adsorption capacity for heavy metal ions.

In this research, the tri-isopropanolamine (TI) was applied to modify the GO and their composite was named as TI-GO. TI contains hydroxyl and nitrogen-containing functional groups. Therefore, it can react with GO easily. Considering the functional groups and low sterically hindered effect, the TI can complex with Pb(II) ions effectively. However, the complex of TI can't be separated from aqueous solutions. Therefore, GO was used as a carrier considering its superior properties. It not only can highly enhance the adsorption capacity of GO but also separate Pb(II) ions from aqueous solutions effectively. Besides, TI-GO can interact with Pb(II) ions through electrostatic attraction since the negative charge on its functional groups. The SEM-EDS, FT-IR, Raman spectra, TG, BET and XPS spectra were applied for characterizing TI-GO and investigating the synthesis and adsorption mechanism of TI-GO. The adsorption experiments were applied to investigate the impact of different factors on the removal of Pb(II) ions using TI-GO, including contact time, initial pH of solution, temperature and initial Pb(II) ions concentration. The adsorption kinetic was researched by pseudo-first-order (PFO) and pseudo-second-order (PSO) models. Langmuir and Freundlich adsorption isotherm models were applied to obtain the adsorption isotherms of TI-GO. Finally, the desorption experiment was investigated to test the re usability of TI-GO.

2. Experiment

2.1. Materials

Graphite was obtained from Henqiu Tech. Inc. TI was purchased from Shanghai Kelin Chemical reagent Co., Ltd. Other chemical reagents were purchased from Sinopharm Chemical Reagent Co., Ltd and Aladdin at analytically pure grade without further treatment.

2.2. Preparation of GO and TI-GO

GO was synthesized by graphite flakes via modified Hummers method [26–28]. Briefly, graphite powders (1 g) and $NaNO_3$ (0.5 g) were stirred with concentrated H_2SO_4 (25 mL). Then the mixture was cooled to below 277 Kin an ice bath. Subsequently, $KMnO_4$ (3 g) was added slowly in 1 h and the temperature of solution should be controlled below 283 K for 2 h. After the $KMnO_4$ was added, the mixture mentioned above was transferred to water bath at 308 K and stirred for 30 min. Then, 80 mL deionized water (DI) was poured slowly to the mixed solution with continuous stirring for 30 min and reacted at 363 K. Subsequently, the reaction was terminated by pouring 60 mL DI water and 15 mL H_2O_2 (30%) solution. 15 min later, 40 mL HCl (10%) was added into suspension. Then, the GO suspension was centrifuged and washed with DI water until the pH of suspension was neutral. Afterward, the obtained brown GO suspension was subjected to ultrasonic-processing and mixed with TI (2.5 g). The mixed solution was stirred for 2.5 h at 358 K and obtained black TI-GO suspension. Subsequently, the TI-GO suspension was filtered and washed with DI water in order to wash out the unreacted TI. Since the suspension which contains TI is alkaline, hence, it can prove that almost all the un-reacted TI has been removed when the pH of suspension is neutral. Finally, the TI-GO was gathered and dissolved in aqueous solutions.

2.3. Characterization of GO and TI-GO

The morphologies and structure of TI-GO and GO were investigated by field emission scanning electron microscopy (FE-SEM) (Mira3, Tescan, Czech Republic) operating at an extra high tension of 20 kV. The surface functional groups of materials were researched by FT-IR spectra (Nicolet 6700, Thermo Electron Scientific Instruments) prepared in KBr pellets. Raman spectroscopy (LabRAM HR800, HORIBA JOBIN YVON S.A.S) was used to investigate the molecular morphology of carbon and its ordered carbon bonding. The XPS (Escalab 250Xi) was applied for investigating the adsorption mechanism of TI-GO. Thermal analysis (STA-449F3) was carried out to explore thermal stability of materials at a heating rate of 10°C/min. Pore size distribution was calculated using Barrett–Joyner–Halenda(BJH) method based on the N_2 adsorption–desorption analysis (ASAP 2020).

2.4. Batch adsorption experiments

TI-GO was applied to remove Pb(II) ions since its various oxygen-containing groups and nitrogen-containing groups. The adsorption experiments have been carried out to evaluate the optimized conditions of adsorption including contact time, initial solution pH, temperature and initial Pb(II) ions concentration. All the adsorption experiments were conducted in 100 mL conical flask in a shaking water bath at 200 rpm. The total volume of Pb(II) ions solution was 50 mL. The solution pH was adjusted by dilute nitric acid. 2.5 mL TI-GO suspension (7 mg TI-GO) was used to remove Pb(II) ions from aqueous solution. After reaching adsorption equilibrium, the adsorption solution was filtered to remove adsorbents and Pb(II) ions concentration was determined using ICP (Optima 5300). Finally, the adsorption capacity of TI-GO was calculated by Eq. (1):

$$Q = \frac{(C_0 - C_e)}{m} \times V \tag{1}$$

where C_e and C_0 (mg/L) are the equilibrium concentration and initial Pb(II) ions concentration, respectively. V(L) represents the total volume of the adsorption solution, m(g) is the dosage of TI-GO.

3. Results and discussion

3.1. Characterization of the GO and TI-GO

Fig. 1 shows the SEM images of GO and TI-GO. GO demonstrated a traditional sheet-like structure with a

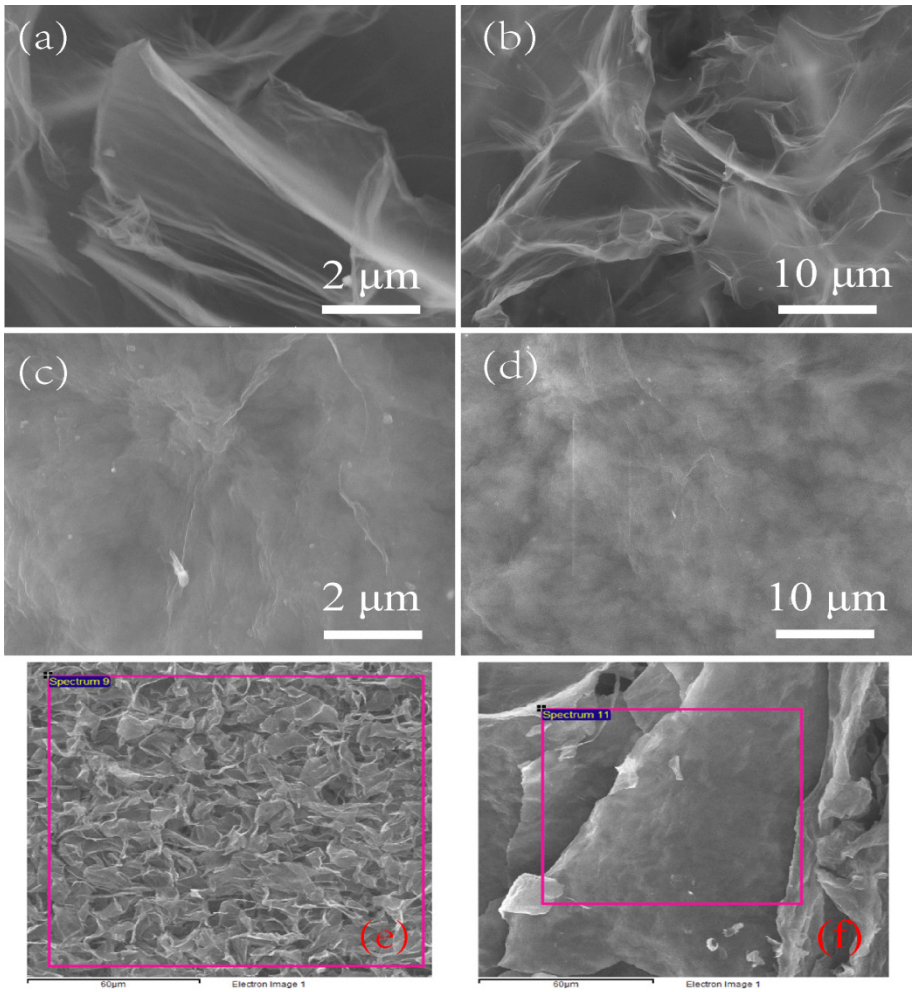

Fig. 1. SEM images of GO (a-b), TI-GO (c-d); EDS area of GO (e), TI-GO (f).

Table 1
The EDS data of GO and TI-GO

GO	Atomic%	TI-GO	Atomic%
C	60.96	C	61.64
O	37.46	O	30.86
N	0.82	N	7.28

smooth surface and wrinkled edge, as the reported literature [29]. The SEM image of TI-GO demonstrated that TI connected on the surface of GO after modification. It indicated that TI has combined with GO. Table 1 lists the EDS data of GO and TI-GO. Based on the EDS results, the GO and TI-GO contain amounts of oxygen atom, which indicated that the GO and TI-GO have abundant oxygen-containing functional groups. Otherwise, the content of nitrogen atoms changed from 0.82% to 7.28% after modification, which indicated that TI has connected with GO as well. Even though, the EDS can't measure the accurate atomic percent whose element number is lower than 14, it still can show the change trend of these elements and prove the synthesis of TI-GO indirectly.

The FTIR patterns of GO and TI-GO are shown in Fig. 2. For GO, the peaks located at 3427.25 and 1718.34 cm^{-1}associated with -OH stretching vibration and C=O stretching vibrations of the –COOH groups, respectively. The peaks located at 1080.30, 1270.63 and 1398.16 cm^{-1} can be assigned to stretching vibration of alkoxy C-O, epoxy C-O and carboxyl O=C-O, respectively [30]. Otherwise, the peak located at 1628.09 cm^{-1} can be assigned to C=C skeletal vibration from unoxidized graphitic domains. These results indicated that GO contains varieties of oxygen-containing functional groups including –COOH, -OH, C-O-C. Compared with GO, TI-GO exhibited new bands at 1336.24 and 1134.78 cm^{-1}, which were the characteristic C-N stretch vibration of TI [31] and C-O-C stretch vibration of ester, respectively. It indicated that the TI combined GO through esterification reaction. After adsorption, the frequency of C=O, C-N and the C-O stretching vibration changed from 1718.30 to 1662.36 cm^{-1}, 1336.24 to 1346.09 cm^{-1}, 1053.87 to 1094.49 cm^{-1}, respectively. Moreover, the intensity of these bands decreased significantly. These results suggested that the TI has combined with GO successfully and the interaction between Pb(II) ions and TI-GO occurs via C=O, C-N and C-O functional groups of TI-GO.

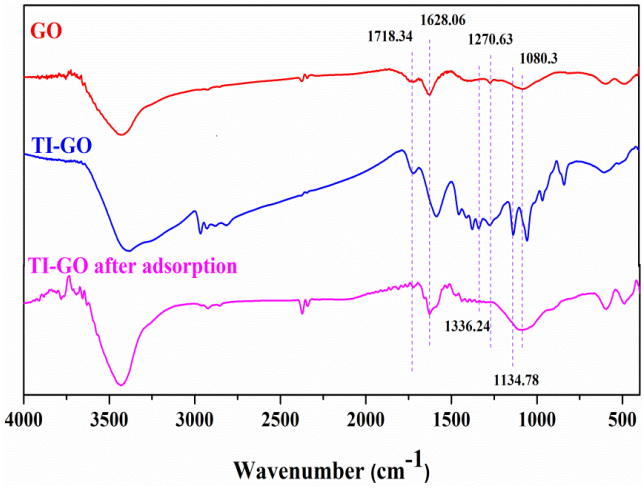

Fig. 2. FTIR spectra of GO, TI-GO and TI-GO after adsorption.

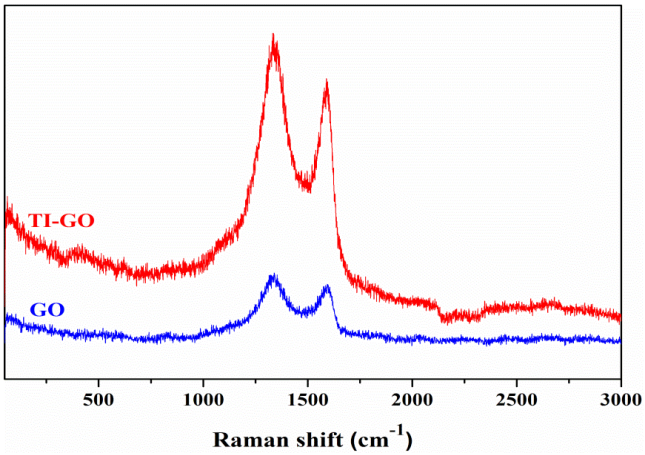

Fig. 3. Raman spectrum of GO and TI-GO.

The Raman spectra of GO and TI-GO are shown in Fig. 3. It shows two characteristic peaks between 1300 and 1600 cm^{-1}, which can be attributed to the D and G bands, respectively. The D band located at approximately 1332 cm^{-1} represented the vibration of defected and disordered sp^3 carbon atoms [32]. In the mean time, the G band showed the first-order scattering of the E_{2g} mode at approximately 1590 cm^{-1}. Compared with GO, the D and G peaks of TI-GO shifted to higher frequencies. The frequency of D band and G band increased from 1332 to 1340 cm^{-1} and 1590 to 1594 cm^{-1}, respectively. According to the calculated intensity ratio of D and G band, the I_D/I_G of TI-GO (1.51) is higher than GO (1.34), which indicated that TI-GO has more graphitic structure defects.

Fig. 4 is the thermogravimetric analysis curve of TI-GO obtained by calcination under N_2 atmosphere. There are two apparent mass reduction in the curve: the mass loss at a temperature below 100°C (373 K) is due to the evaporation of the residual water and surface adsorbed water in the sample; then the mass begins to decrease sharply, due to the decomposition of the GO in the complex. When the temperature is greater than 600°C (873 K), the curve tends

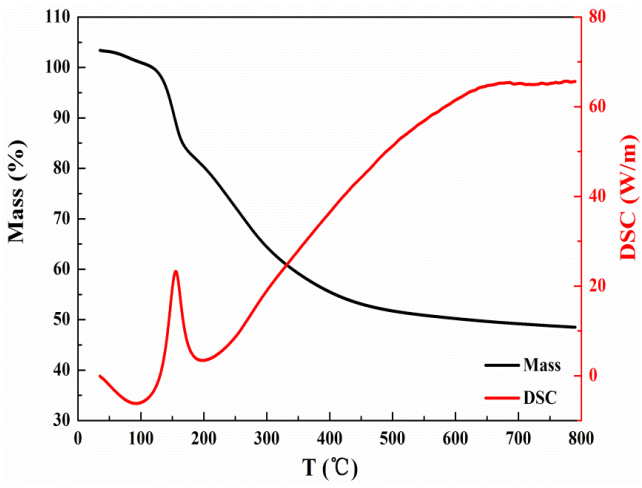

Fig. 4. TG-DSC thermogram of TI-GO.

to be gentle, indicating that GO has completely decomposed. The remaining 48% is the mass percentage of TI in the composite.

Nitrogen adsorption–desorption isotherms and pore volume distribution are shown in Fig. 5. Nitrogen adsorption–desorption isotherm can be classified as type IV isotherm with hysteresis loop for mesoporous materials. Brunauer–Emmett–Teller (S_{BET}) specific surface area, cumulative pore volume (P_{vol}) and average pore size diameter (P_{size}) are shown in Table 2. The BET surface area of TI-GO was 5.58 m^2/g, which is attributed to the severe cross-linking of organic TI on the surface of GO.

3.2. Adsorption studies

3.2.1. Effect of contact time

The effect of contact time on the removal of Pb(II) ions is shown in Fig. 6A. The initial Pb(II) ions concentration varied from 100–300 mg/L. Otherwise, the GO was applied to remove 300 mg/L Pb(II) ions from aqueous solution. The experiment results showed that the adsorption capacity of TI-GO increased rapidly in 10 min. After 10 min, the adsorption capacity changed little. It can be explained by the rapid diffusion of Pb(II) ions toward to the external surface of TI-GO. The subsequent slow adsorption process can be explained by the long diffusion range of adsorbed Pb(II) ions into inner sites of TI-GO [33]. It illustrated that the adsorption capacity of TI-GO can reach adsorption equilibrium in 10 min. Moreover, the adsorption curve of GO indicated that the equilibrium adsorption capacity of GO is 216.8 mg/g, which indicated that the TI-GO has significantly increased the adsorption capacity of GO.

3.2.2. Effect of initial pH

Fig. 6B shows the effect of initial solution pH on the removal of Pb(II) ions using TI-GO. The initial pH of adsorption solution was adjusted by dilute HNO_3 and the pH was in the range of 1.0–5.0. The adsorption capacity of TI-GO sharply increased from 101.1 to 1344.6 mg/g

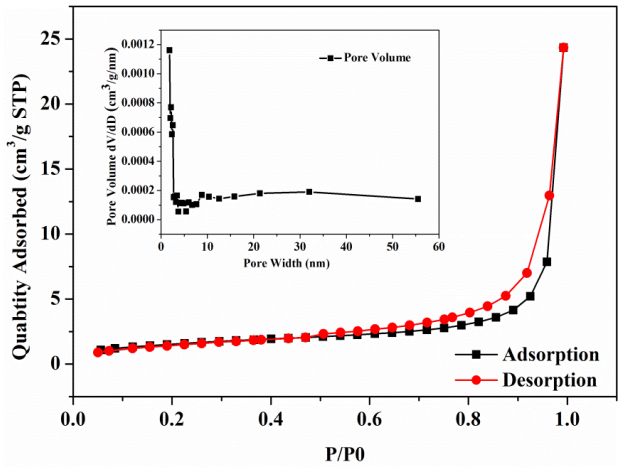

Fig. 5. Nitrogen adsorption/desorption isotherms and pore volume distribution of TI-GO.

Table 2
Structural properties of TI-GO

Adsorbent	TI-GO
S_{BET} (m^2/g)	5.578
P_{vol} (cm^3/g)	0.037
P_{size} (nm)	22.354

with the increase of initial solution pH. This phenomenon suggested that the surface charge of TI-GO is positive at lower pH and the adsorption process of TI-GO is affected by the competitive adsorption between H^+ and Pb(II) ions. With the increase of initial solution pH, the protons concentration highly decreased and the adsorption capacity of TI-GO sharply increased. It can be explained by the change in ionization state of carboxyl, hydroxyl and nitrogen-containing functional groups [34]. The –COOH on the surface of adsorbent can be transformed to $–COO^-$, which can enhance the electrostatic effect between Pb(II) ions and adsorbent. Not only that, the protonation degree of nitrogen-containing groups decreased with the increase of pH, which can improve the chelating ability of TI-GO for Pb(II) ions [35]. Moreover, since Pb(II) ions can start to hydrolyze when the pH of adsorption solution excess 5.2. Therefore, the adsorption experiment didn't carry out at pH higher than 5.2.

3.2.3. Effect of temperature

Fig. 6C shows the effect of temperature on the removal of Pb(II) ions using TI-GO. The adsorption capacity of TI-GO decreased from 747 to 604 mg/g with the rising temperature. It suggested that the adsorption of Pb(II) ions onto TI-GO is an exothermic process.

To further investigate the effect of temperature, the thermodynamic parameters (ΔG^0, ΔS^0 and ΔH^0) were calculated to study the spontaneity and thermal properties during

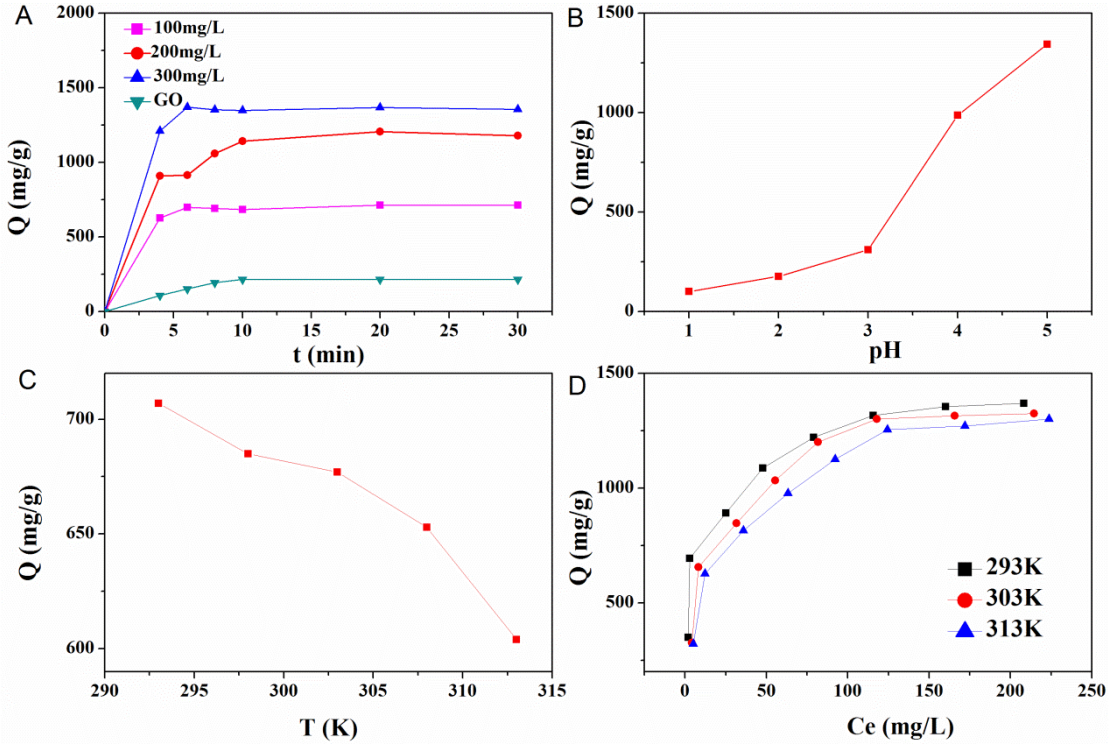

Fig. 6. (A) The effect of contact time on the removal of Pb(II) ions (adsorbent dose 7 mg; temperature 303 K; pH 5.0; contact time 30 min). (B) The effect of initial pH on the removal of Pb(II) ions (adsorbent dose 7 mg; Pb(II) ions concentration 300 mg/L ; temperature 303 K; contact time 30 min). (C) The effect of temperature on the removal of Pb(II) ions (adsorbent dose 7 mg; Pb(II) ions concentration 100 mg/L; pH 5.0; contact time 30 min) (D) The effect of initial Pb(II) ions concentration on the removal of Pb(II) ions (adsorbent dose 7 mg; pH 5.0; contact time 30 min).

adsorption process. The Gibbs free energy (ΔG^0) can be calculated by Eq. (2).

$$\Delta G^0 = -RT \ln K^0 = \Delta H^0 - T\Delta S^0 \quad (2)$$

where R and T are the ideal gas constant (8.314 J/(mol K)) and Kelvin temperature (K), respectively. Then, the enthalpy (ΔH^0) and entropy (ΔS^0) can be calculated by the slope and intercept of Eq. (3). Eq. (4) shows the equation of K_D.

$$\ln K_D = \frac{\Delta S^0}{R} - \frac{\Delta H^0}{RT} \quad (3)$$

$$K_D = \frac{Q_e}{C_e} \quad (4)$$

where K_D is the adsorption equilibrium constant. Fig. 7 shows the fitting results of Eq. (3). Table 3 lists the calculated thermodynamic parameters. The negative ΔG^0 proved that the adsorption process of Pb(II) ions onto TI-GO is spontaneous. Besides, the absolute value of ΔG^0 decreases with the rising temperature, which also indicated the lower temperature is benefit to the adsorption process. The negative value of ΔH^0 (–110.51 kJ/mol) and ΔS^0 (–0.323 kJ/(mol·K) revealed an exothermic adsorption process. Therefore, the results of thermodynamic research also indicated that the adsorption of Pb(II) ions using TI-GO is a spontaneous exothermic process.

3.2.4. Effect of initial concentration

The effect of initial Pb(II) ions concentration was carried out at pH 5.0 and the initial concentration was varied from 50 to 400 mg/L. As shown in Fig. 6D, the adsorption capacity of TI-GO increased rapidly with the rise of Pb(II) ions concentration at the beginning, then changed little at higher concentration. It suggested that the active adsorption sites of TI-GO surface are saturated at higher concentration.

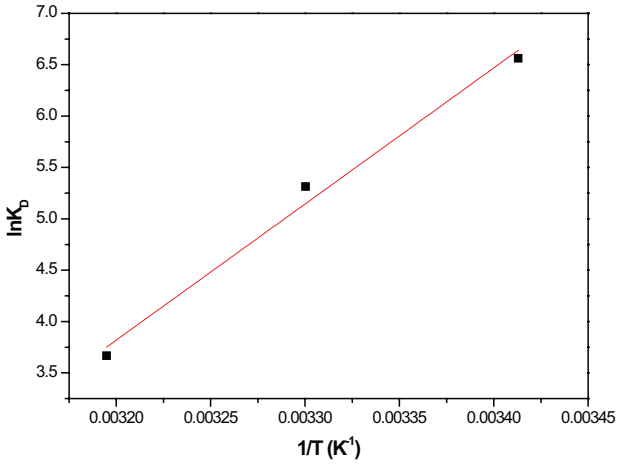

Fig. 7. The linear fit plot of ln K_D vs 1/T.

Table 3
Thermodynamic parameters of the adsorption process

Temperature	ΔG^0 (kJ/mol)	ΔH^0 (kJ/mol)	ΔS^0 (kJ/(mol·K))
293 K	–15.87		
303 K	–12.64	–110.51	–0.323
313 K	–9.411		

3.3. Adsorption kinetics

The kinetic data were fitted by PFO [36] and PSO [37] kinetic models. The linear equations of PFO and PSO models are shown in Eq. (5) and Eq. (6), respectively:

$$\ln(q_e - q_t) = \ln q_e - k_f \times t \quad (5)$$

$$\frac{t}{q_t} = \frac{1}{k_s \times q_e^2} + \frac{t}{q_e} \quad (6)$$

where q_e and q_t (mg/g) are the adsorption capacity of TI-GO at equilibrium and instantaneous, respectively. The k_f and k_s represent the kinetics rate constant of PFO and PSO, respectively. Figs. 8A and 8B show the fitting results of these two models, respectively. The calculated kinetic parameters are listed in Table 4. The fitting results proved that the adsorption kinetic of TI-GO fit the PSO model better. The correlation coefficient of PSO kinetic curves ($R^2 > 0.996$) is much higher than PFO kinetic model ($R^2 < 0.855$). Otherwise, the q_e calculated from PSO kinetic model is similar to the experimental q_e, which can also prove the fitting results. Therefore, the adsorption kinetic research suggested that the adsorption process of Pb(II) ions onto TI-GO is mainly controlled by the chemical interaction between the binding sites of adsorbents and Pb(II) ions.

3.4. Adsorption isotherms

To further investigate the adsorption process, the Langmuir and Freundlich adsorption isotherm models were applied to investigate the adsorption mechanism. Eq. (7) and Eq. (8) show the Langmuir and Freundlich adsorption models, respectively:

$$\frac{C_e}{Q_e} = \frac{1}{Q_m \times K_L} + \frac{C_e}{Q_m} \quad (7)$$

$$\ln Q_e = \ln K_f + \frac{1}{n} \ln C_e \quad (8)$$

where C_e (mg/L) and Q_e (mg/g) are the equilibrium Pb(II) ions concentration and the adsorption capacity of TI-GO, respectively. Q_m (mg/g) represents the theoretical maximum adsorption capacity. K_L (L/mg) is the constant, which relates to the heat of sorption. K_f (mg g^{-1} (L $mg^{-1})^{1/n}$) is a constant representing the adsorption capacity. The *1/n* represents the optimal adsorption isotherm when the *1/n* is lower than 0.5. Figs. 8C and 8D show the Langmuir and Freundlich adsorption isotherm curve, respectively. Table 5 lists the relative parameters of adsorption isotherm models. The linear correlation coefficient of Langmuir ($R^2 > 0.994$) was much higher than Freundlich ($R^2 < 0.948$), which indicated that the adsorption isotherms fitted Langmuir adsorption isotherm model better. It suggested that the adsorption process

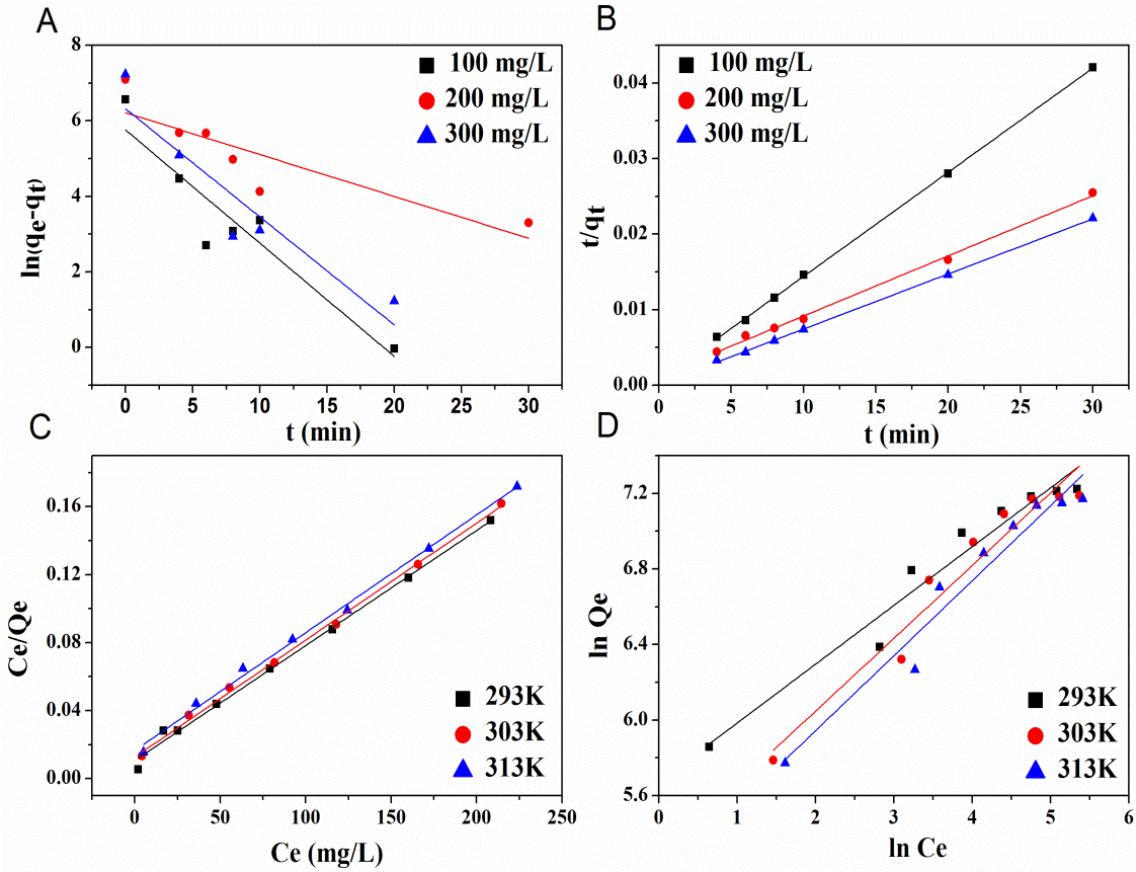

Fig. 8. (A) PFO kinetic model of TI-GO (B) PSO kinetic model of TI-GO (C) Langmuir adsorption isotherm model of TI-GO (D) Freundlich adsorption isotherm model of TI-GO.

Table 4
Parameters of the kinetic models for Pb(II) ions adsorption on TI-GO

Kinetic models		100 mg/L	200 mg/L	300 mg/L
PFO	q_e (mg/g)	315.9	499.6	554.34
	k_f	0.299	0.111	0.286
	R^2	0.855	0.712	0.839
PSO	q_e (mg/g)	724.6	1256.3	1370.9
	$k_s \times 10^{-3}$	3.06	0.528	3.7
	R^2	0.999	0.996	0.999

Table 5
Parameters of Langmuir and Freundlich models for Pb(II) ions adsorption on TI-GO

	Langmuir			Freundlich		
	K_L	Q_m	R^2	ln K_f	$1/n$	R^2
293 K	0.063	1478	0.994	5.67	0.311	0.948
303 K	0.054	1453	0.997	5.27	0.385	0.933
313 K	0.042	1443	0.996	5.14	0.396	0.943

of Pb(II) ions using TI-GO is a homogeneous mono layer adsorption and the affinity of adsorption sites on the adsorbent to adsorbate is equal [38]. Moreover, the Q_m calculated by Langmuir model at 293 K is estimated to be 1478 mg/g. It suggested that the TI-GO is a promising adsorbent material for the removal of Pb(II) ions.

3.5. Compared with other adsorbents

There are many adsorbents have been applied for the removal of Pb(II) ions from aqueous solutions. For comparison, the adsorption capacities of different GO and modified GO materials for the removal of Pb(II) ions is listed in Table 6. The results showed that the adsorption capacity of TI-GO are much higher than other GO based adsorbents, which means the TI is a promising molecule for the functionalized of GO.

3.6. Synthesis and adsorption mechanism of TI-GO

The XPS analysis has been applied for investigating the synthesis and adsorption mechanism of TI-GO. The wide XPS spectra of TI-GO and TI-GO after adsorption are shown in Fig.9.The XPS spectra of TI-GO mainly show the C1s, N 1s and O 1s peaks. The XPS analysis of C1s spectra shows that there are three main types of carbon

species in TI-GO including C-C/C=C (284.13 eV), C-O/C-N (285.9 eV) and C=O (287.79 eV). The ratios of C-C/C=C, C-O/C-N, and C=O were 51%, 44%, and 5% respectively,which indicated that the TI-GO contains abundant oxygen-containing functional groups. The peaks of N1s at 398.45 eV, 399.34 eV and 401.29 eV can be assigned to the C-N of TI, which combined with GO through carboxyl group, epoxy group and hydroxyl group, respectively. The ratio of each peak were 38%(398.45 eV),4% (399.34 eV),58%(401.29 eV) , respectively. It indicated TI combined the GO through these functional groups. The peaks of O1s at 531.77 eV, 529.99 eV and 533.82 eV corresponding to O-H, C=O and epoxy group, respectively. The ratios of O-H, C=O, and epoxy group were 90%, 9%, and 1% respectively. Compared with TI-GO, the binding energy of TI-GO after adsorption shifted to higher value. It illustrated the Pb(II) ions complex with TI-GO through nitrogen and oxygen-containing functional groups. Moreover, the new peaks located at 406.84 eV and 532.44 eV corresponding to the $-N^{+}-O^{-}$ of NO_3^-. Moreover, the full scale XPS survey of TI-GO after adsorption shows two high intense peaks at 139.25 eV and 142.6 eV can be assigned to the Pb (II) binding energies for the $4f_{7/2}$ and $4f_{5/2}$ orbital, which are associated with the presence of chelation and Pb-O bonding.Fig. 10 shows the synthesis and adsorption models of GO and TI-GO.

Table 6
The adsorption capacity of Pb(II) ions on different GO and modified GO materials

Adsorbents	Q_m (mg/g)	Temperature (K)	References
GO	125	298	[39]
$CSGO_5$	216	303	[40]
GOMO	190	303	[41]
Gr-CBr_2	49	298	[42]
EDTA-mGO	508	318	[43]
GO-SBA-15 GO-HPEI1.8K gel	255	298	[6]
TI-GO	438	288	[34]
	1478	293	This work

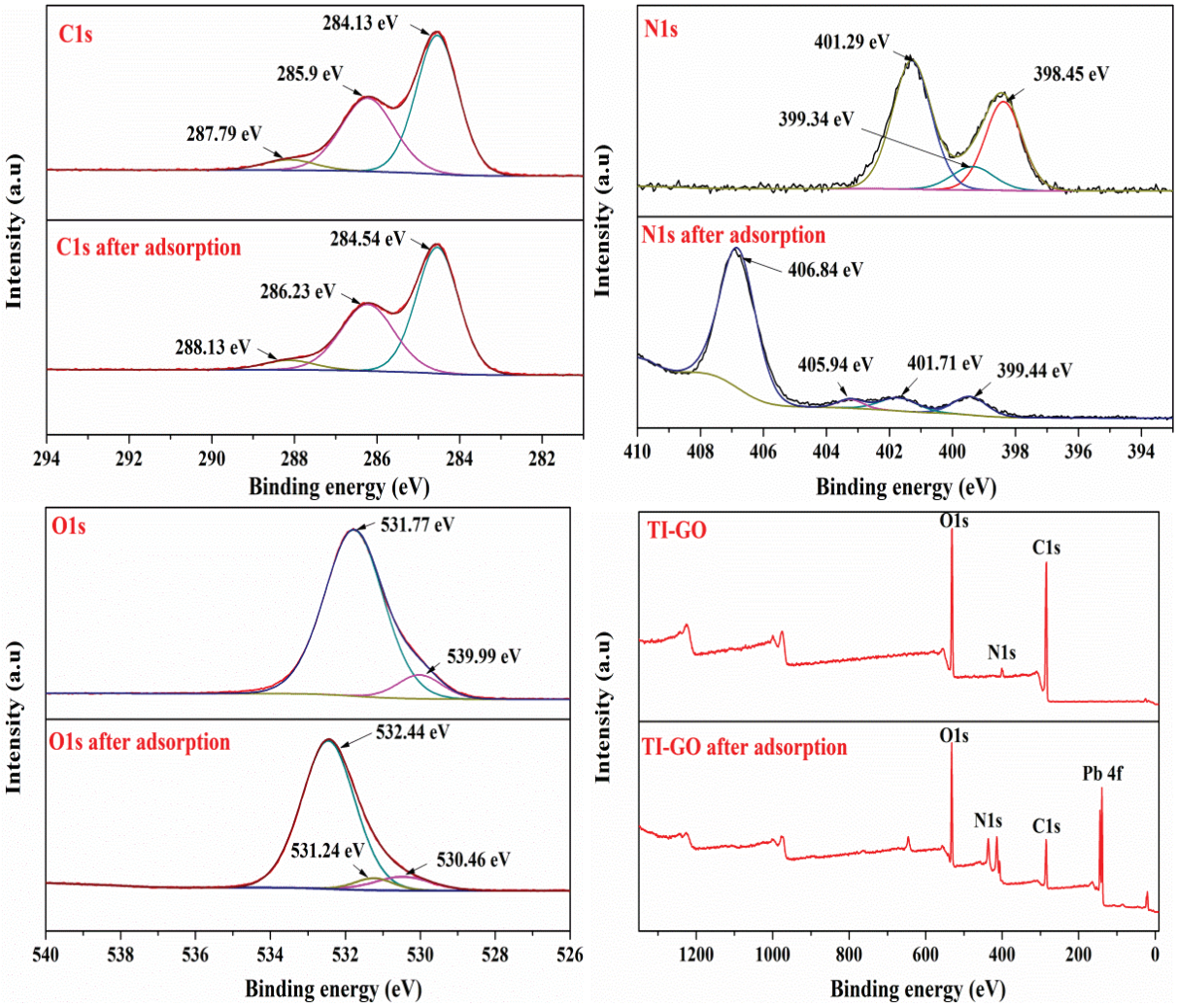

Fig. 9. X-ray photoelectron spectroscopy spectra of TI-GO and TI-GO after adsorption.

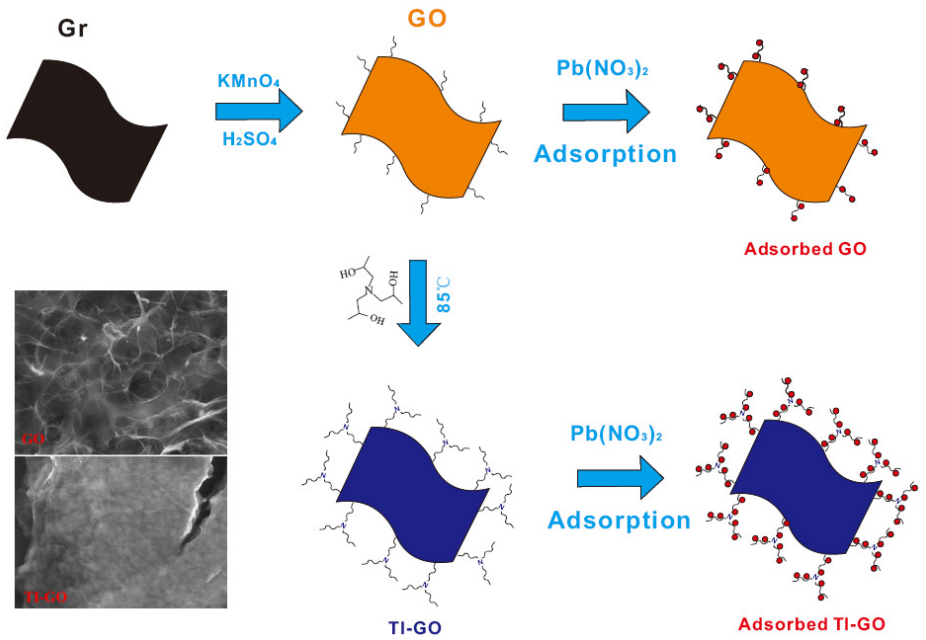

Fig. 10. The synthesis and adsorption models of GO and TI-GO.

3.7. Desorption

The adsorption experiment carried out at 303 K and pH 5.0. After adsorption, the Pb(II) ions concentration decreased from 300 mg/L to 118 mg/L. Then, the adsorbents were desorbed in dilute nitric acid solution (pH 1.0). During desorption process, the volume of dilute nitric acid solution was the same as adsorption process. Finally, Pb(II) ions concentration increased from 118 mg/L to 290 mg/L, which suggested that the dilute nitric acid solution can desorb Pb(II) ions from TI-GO effectively. By calculation, the desorption rate was 94.5%.

4. Conclusions

In this study, the TI-GO was synthesized by simple one-step reaction and characterized by SEM-EDS, FT-IR, Raman spectra, TG, BET and XPS. The characterization results indicated TI-GO was synthesized successfully and TI-GO adsorbed Pb(II) ions through the complexation effect between Pb(II) ions and the functional groups on TI-GO. Batch adsorption experiment showed that the TI-GO can reach adsorption equilibrium in 30 min and get maximum adsorption capacity at pH 5.0, 293 K. The thermodynamic research illustrated that the adsorption of Pb(II) ions using TI-GO is a spontaneous exothermic process. Moreover, the adsorption kinetic and adsorption isotherm research indicated that the adsorption process of Pb(II) ions fit the PSO kinetic and Langmuir adsorption isotherm model. Besides, the Q_m evaluated by Langmuir adsorption isotherm is 1478 mg/g. Finally, the result of desorption experiment showed that the Pb(II) ions can be desorbed by dilute nitric acid solution effectively. All in all, the research results show that the TI-GO is a promising adsorbent material for the removal of Pb(II) ions from aqueous solution.

Acknowledgement

This research was supported by the Hunan Provincial Science and Technology Plan Project (No.2016TP1007), the National Natural Science Foundation of China (No.21776320) and Hunan Provincial Natural Science Foundation of China (No.2018JJ2489, No.2018JJ2484), the Open-End Fund for the Valuable and Precision Instruments of Central South University (No.CSUZC201827).

References

[1] G. Zhao, J. Li, X. Ren, C. Chen, X. Wang, Few-layered graphene oxide nanosheets as superior sorbents for heavy metal ion pollution management, Environ. Sci. Technol., 45 (2011) 10454–10462.
[2] Z.H. Huang, X. Zheng, W. Lv, M. Wang, Q.H. Yang , F. Kang, Adsorption of lead(II) ions from aqueous solution on low-temperature exfoliated graphene nanosheets, Langmuir, 27 (2011) 7558–7562.
[3] G. Garcíarosales, A. Colíncruz, Biosorption of lead by maize (Zea mays) stalk sponge, J. Environ. Manage., 91 (2010) 2079–2086.
[4] J. Feng, Z. Yang, G. Zeng, J. Huang, H. Xu, Y. Zhang, S. Wei, L. Wang, The adsorption behavior and mechanism investigation of Pb(II) removal by flocculation using microbial flocculant GA1, Bioresour. Technol., 148 (2013) 414–421.
[5] M.M. Matlock, B.S.H. And, D.A. Atwood, Chemical precipitation of lead from lead battery recycling plant wastewater, Ind. Eng. Chem. Res., 41 (2002) 1579–1582.
[6] S. Li, Y. Wei, Y. Kong, Y. Tao, C. Yao, R. Zhou, Electrochemical removal of lead ions using paper electrode of polyaniline/attapulgite composites, Synthetic. Met., 199 (2015) 45–50.
[7] C. Duran, V.N. Bulut, A. Gundogdu, D. Ozdes, N. YïLdïRïM, M. Soylak, H.B. Senturk, L. Elci, Carrier element-free coprecipitation with 3-phenly-4-o-Hydroxybenzylidenamino-4, 5-dihydr -o-1, 2, 4-triazole-5-oneforseparation/preconcentration of Cr(III), Fe(III), Pb(II) and Zn(II) from aqueous solutions, J. Hazard. Mater., 167 (2009) 294–299.

[8] S. Koushkbaghi, P. Jafari, J. Rabiei, M. Irani, M. Aliabadi, Fabrication of PET/PAN/GO/Fe_3O_4 nanofibrous membrane for the removal of Pb(II) and Cr(VI) ions, Chem. Eng. J., 301 (2016) 42–50.
[9] G. Ming, H. Duan, M. Xia, G. Sun, W. Sun, Y. Liu, L. Lucia, A novel fabrication of mono disperse melamine–formaldehyde resin microspheres to adsorb lead (II), Chem. Eng. J., 288 (2016) 745–757.
[10] S.C. Liu, J.M. Pan, Y. Ma, F.X. Qiu, X.H. Niu, T. Zhang, L.I. Yang, Three-in-one strategy for selective adsorption and effective separation ofcis-diol containing luteolin from peanut shell coarse extract using PU/GO/BA-MOF composite, Chem. Eng. J., 306 (2016) 655–666.
[11] D. Gu, J.B. Fein, Adsorption of metals onto graphene oxide: Surface complexation modeling and linear free energy relationships, Colloid. Surfaces. A., 481 (2015) 319–327.
[12] W.T. Tsai, C.W. Lai, T.Y. Su, Adsorption of bisphenol-A from aqueous solution onto minerals and carbon adsorbents, J. Hazard. Mater., 134 (2006) 169–175.
[13] B. Socasrodríguez, A.V. Herreraherrera, M. Asensioramos, J. Hernándezborges, Recent applications of carbon nanotube sorbents in analytical chemistry, J. Chromatogr. A ., 1357 (2014) 110–146.
[14] V.K. Gupta, R. Kumar, A. Nayak, T.A. Saleh, M.A. Barakat, Adsorptive removal of dyes from aqueous solution onto carbon nanotubes: a review, Adv. Colloid. Interface., 24 (2013) 193–194.
[15] A. Pahlavan, V.K. Gupta, A.L. Sanati, F. Karimi, M. Yoosefian, M. Ghadami, ZnO/CNTs nanocomposite/ionic liquid carbon paste electrode for determination of noradrenaline in human samples, Electrochim. Acta., 123 (2014) 456–462.
[16] N. Chen, J. Teng, F.P. Jiao, X.Y. Jiang, X.H. Hao, J.G. Yu, Preparation of triethanolamine functionalized carbon nanotube for aqueous removal of Pb(II), Desal. Water. Treat., 271 (2017) 191–200.
[17] Y. Xie, J. Song, P. Zhou, Y. Ling, Y. Wu, Controllable Synthesis of TiO_2/graphene nanocomposites for long lifetime lithium storage: nanoparticles vs. nanolayers, Electrochim. Acta., 210 (2016) 358–366.
[18] M. Naushad, T. Ahamad, G. Sharma, A.A.H. Al-Muhtaseb, A.B. Albadarin, M.M. Alam, Z.A. Alothman, S.M. Alshehri, A.A. Ghfar, Synthesis and characterization of a new starch/SnO_2 nanocomposite for efficient adsorption of toxic Hg^{2+} metal ion, Chem. Eng. J., 300 (2016) 306–316.
[19] R. Rostamian, H. Behnejad, A comparative adsorption study of sulfamethoxazole onto graphene and graphene oxide nanosheets through equilibrium, kinetic and thermodynamic modeling, Process. Saf. Environ., 102 (2016) 20–29.
[20] W. Cai, R.D. Piner, F.J. Stadermann, S. Park, M.A. Shaibat, Y. Ishii, D. Yang, A. Velamakanni, S.J. An, M. Stoller, Synthesis and solid-state NMR structural characterization of 13C-labeled graphite oxide. Science., 321 (2008) 1815–1817.
[21] X. Liu, J. Li, X. Wang, C. Chen, X. Wang, High performance of phosphate-functionalized graphene oxide for the selective adsorption of U(VI) from acidic solution, J. Nucl. Mater., 466 (2015) 56–64.
[22] R. Zare-Dorabei, S.M. Ferdowsi, A. Barzin, A. Tadjarodi, Highly efficient simultaneous ultrasonic-assisted adsorption of Pb(II), Cd(II), Ni(II) and Cu(II) ions from aqueous solutions by graphene oxide modified with 2,2-dipyridylamine: Central composite design optimization, Ultrason. Sonochem., 32 (2016) 265–276.
[23] G.G. Liu, S. Gui, H. Zhou, F.T. Zeng, Y.H. Zhou, H.Q. Ye, A strong adsorbent for Cu^{2+}: graphene oxide modified with triethanolamine, Dalton Trans., 43 (2014) 6977–6980.
[24] H. Yan, H. Yang, A. Li, R. Cheng, pH-tunable surface charge of chitosan/graphene oxide composite adsorbent for efficient removal of multiple pollutants from water, Chem. Eng. J., 284 (2016) 1397–1405.
[25] D. Shao, G. Hou, J. Li, W. Tao, X. Ren, X. Wang, PANI/GO as a super adsorbent for the selective adsorption of uranium(VI), Chem. Eng. J., 255 (2014) 604–612.
[26] W.S.H. Jr, R.E. Offeman, Preparation of Graphitic Oxide, J. Am. Chem. Soc., 80 (1958) 1339.
[27] J. Teng, X. Zeng, X. Xu, J.G. Yu, Assembly of a novel porous 3D graphene oxide-starch architecture by a facile hydrothermal method and its adsorption properties toward metal ions, Mater. Lett., 214 (2018) 31–33.
[28] X. Zeng, J. Teng, J.G. Yu, A.S. Tan, D.F. Fu, H. Zhang, Fabrication of homogeneously dispersed graphene/Al composites by solution mixing and powder metallurgy, Int. J. Min. Met. Mater., 25 (2018) 102–109.
[29] Y. Sun, D. Shao, C. Chen, S. Yang, X. Wang, Highly efficient enrichment of radio nuclides on graphene oxide-supported polyaniline. Environ. Sci. Technol., 47 (2013) 9904–9910.
[30] J. Wang, X. Wen, F. Yang, Z.F. Cao, S. Wang, H. Zhong, Preparation of a novel two-dimensional carbon material and enhancing Cu(II) ions removal by phytic acid, Environ. Earth. Sci., 77 (2018) 472–482.
[31] J. Tian, F. Gao, X.Q. Yu, W. Wu, H. Meng, Preparation of nitrogen-doped graphene by high-gravity technology and its application in oxygen reduction. Particuology., 34 (2017) 110–117.
[32] R.W. Havener, S.Y. Ju, L. Brown, Z.H. Wang, M. Wojcik, C.S. Ruiz-Vargas, J. Park, High-throughput graphene imaging on arbitrary substrates with wide field Raman spectroscopy, ACS Nano., 6 (2012) 373–380.
[33] X. Wang, Z. Chen, X. Wang, Graphene oxides for simultaneous highly efficient removal of trace level radio nuclides from aqueous solutions, Sci. Chin. Chem., 58 (2015) 1766–1773.
[34] L. Yi, X. Li, J. Liu, X. Liu, C. Chen, G. Li, Y. Meng, Graphene oxides cross-linked with hyperbranched polyethylenimines: Preparation, characterization and their potential as recyclable and highly efficient adsorption materials for lead(II) ions, Chem. Eng. J., 285 (2016) 698–708.
[35] H. Cui, Q. Yan, Q. Li, Q. Zhang, J. Zhai, Adsorption of aqueous Hg(II) by a polyaniline/attapulgite composite, Chem. Eng. J., 211 (2012) 216–223.
[36] Y. Sun, S. Yang, G. Sheng, Z. Guo, X. Wang, The removal of U(VI) from aqueous solution by oxidized multi walled carbon nanotubes, J. Environ. Radioactiv., 105 (2012) 40–47.
[37] Y.S. Ho, G. Mckay, Pseudo-second order model for sorption processes, Process. Biochem., 34 (1999) 451–465.
[38] T.X. Hai, H.C. Jian, S. Xue, H.H. Yi, B.S. Zhen, R.H. Shi, W. Wen, S.X. Li, X.G. Hong, B.W. Wen, NH2-rich polymer/graphene oxide use as a novel adsorbent for removal of Cu(II) from aqueous solution, Chem. Eng. J., 263 (2015) 280–289.
[39] X.M. Huang, M. Pan, The highly efficient adsorption of Pb(II) on graphene oxides: A process combined by batch experiments and modeling techniques, J. Mol. Liq., 215 (2016) 410–416.
[40] L. L, C. Li, C.L. Bao, Q. Jia, P.F. Xiao, X.T. Liu, Q.P. Zhang, Preparation and characterization of chitosan/graphene oxide composites for the adsorption of Au(III) and Pd(II). Talanta., 93 (2012) 350–357.
[41] S. Mohan, V. Kumar, D.K. Singh, S.H. Hasan, Effective removal of lead ions using graphene oxide-MgO nanohybrid from aqueous solution: Isotherm, kinetic and thermodynamic modeling of adsorption. J. Environ. Chem. Eng., 5 (2017) 2259–2273.
[42] T. Jie, Z. Xiang, Y.B. Yu, X.H. Zhao, Z.H. Wang, J.G. Yu, X.M. Xu, M. Zhong, X.W. Wu, W.X. Zhou, Z. Zhou, Dibromocarbene modified graphene: preparation, characterization and its application in removal of Pb(II) from aqueous solutions, Nanosci. Nanotech. Let., 8 (2016) 226–231.
[43] L.M. Cui, Y.G. Wang, L. Gao, L.H. Hu, L.G. Yan, Q. Wei, B. Dua, EDTA functionalized magnetic graphene oxide for removal of Pb(II), Hg(II) and Cu(II) in water treatment: Adsorption mechanism and separation property. Chem. Eng. J., 281 (2015) 1–10.